Journal of Molecular Graphics and Modelling 28 (2009) 54–61

Contents lists available at ScienceDirect

Journal of Molecular Graphics and Modelling

journal homepage: www.elsevier.com/locate/JMGM

# Pharmacophore and docking-based combined *in-silico* study of KDR inhibitors

F.A. Pasha [c,1], M. Muddassar [c,d], M.M. Neaz [c,d], Seung Joo Cho [a,b,*]

[a] Research Center for Resistant Cells, Chosun University, Gwangju 501-759, Republic of Korea
[b] College of Medicine, Chosun University, 375 Seosuk-dong, Dong-gu, Gwangju 501-759, Republic of Korea
[c] Computational Science Center, Future Fusion Technology Division, Korea Institute of Science and Technology, PO Box 131, Seoul 130-650, Republic of Korea
[d] University of Science and Technology ,113 Gwahangno. Yuseong-gu. Daejeon. Korea

ARTICLE INFO

*Article history:*
Received 25 September 2008
Received in revised form 22 March 2009
Accepted 11 April 2009
Available online 19 April 2009

*Keywords:*
3D-QSAR
Drug design
Pharmacophore
Docking
CoMFA
CoMSIA
VEGFR

ABSTRACT

The growth and metastasis of solid tumors is dependent on angiogenesis. The vascular endothelial growth factor (VEGF) and its cell surface receptor in human KDR (kinase domain containing receptor or VEGFR-2) have particular interest because of their importance in angiogenesis. The development of novel inhibitors of VEGFR-2 would be helpful to check the growth of tumors. Quantitative structure activity relationship (QSAR) analyses used to understand the structural factors affecting inhibitory potency of thiazole-substituted pyrazolone derivatives. Several pharmacophore-based models indicated the importance of steric, hydrophobic and hydrogen bond acceptor groups to inhibitory activity. The comparative molecular field analyses (CoMFA) and comparative molecular similarity indices analyses (CoMSIA) based 3D-QSAR models were derived using pharmacophore-based alignment. Both CoMFA ($q^2 = 0.70$, $r^2 = 0.97$ and $r^2_{predictive} = 0.61$) and CoMSIA ($q^2 = 0.54$, $r^2 = 0.82$ and $r^2_{predictive} = 0.66$) gave reasonable results. The molecular docking (receptor-guided technique) with a recently reported receptor structure (PDB = 1YWN) were performed. The docked alignment was subsequently used for 3D-QSAR (CoMFA; $q^2 = 0.56$, $r^2 = 0.97$, $r^2_{predictive} = 0.82$, CoMSIA; $q^2 = 0.58$ $r^2 = 0.91$, $r^2_{predictive} = 0.69$). The overall both studies were indicated, steric, electrostatic and hydrogen bond acceptor effects contribute to the inhibitory activity. CoMFA and CoMSIA models suggested that a positive bulk with hydrophobic effect is desirable around position 4 and 5 and hydrogen bond acceptor groups around pyrazolones ring will be helpful.



## 1. Introduction

Angiogenesis is a physiological process involving the growth of new blood vessels from pre-existing vessels. It occurs during tissue growth from embryonic development to maturity, after which the process enters a period of relative quiescence during adulthood. Angiogenesis is also activated during wound healing and at certain stages of the female reproductive cycle [1]. One of the most extensively studied pathways in this area is vascular endothelial growth factor (VEGF) [2] and its cell surface receptor in human KDR (kinase domain containing receptor or VEGFR-2) [3,4] due to their important roles in angiogenesis [5]. This is vital for survival and proliferation of tumor cells. KDR receptors, shown to be expressed primarily in endothelial cells [6] upon binding to VEGF, get activated and their intracellular kinase domains undergo auto-phosphorylation, which in turn triggers signaling pathways leading to sprouting of blood vessels toward the tumor cells. Therefore, inhibition of KDR kinase and subsequent blockage of angiogenesis could be an alternate approach to cancer therapy. Several small molecular VEGFR-2 inhibitors [7,8] have emerged as promising anti-angiogenic agents for possible treatment against a wide variety of cancers [9]. One of the pioneering class of compounds belongs to 1,2,3-thiadiazole substituted pyrazolones. To explore further possibilities we used different quantitative structure activity relationship (QSAR) techniques, which are also in our practice [10–15]. The current study deals ligand-based and receptor-guided QSAR techniques. The ligand-based study was performed using pharmacophore techniques with PHASE module [16] and the receptor-guided study was performed using molecular docking techniques with GLIDE. A recently reported co-crystal structure (1YWN) [17] obtained from protein data bank and used as receptor structure. Additionally the 3D-QSAR (comparative molecular field analysis (CoMFA) and comparative

* Corresponding author.
*E-mail addresses:* fpasha@rediffmail.com (F.A. Pasha), chosj@chosun.ac.kr (S.J. Cho).
[1] Current Address: Institute de Biologie Structurale, 41, rue Jules horowitz, Grenoble-Cedex-38027, France.

1093-3263/$ – see front matter © 2009 Elsevier Inc. All rights reserved.
doi:10.1016/j.jmgm.2009.04.006

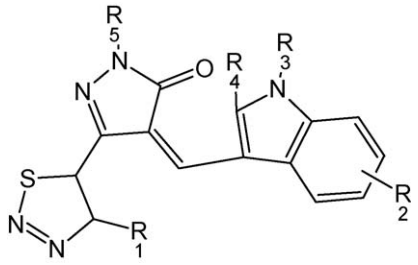

**Fig. 1.** The basic skeleton of pyrazolone compounds.

molecular similarity indices analysis (CoMSIA)) [18,19] have been performed to understand the possible interaction involved in ligand binding with KDR.

## 2. Material and methods

### 2.1. Data sets

Fig. 1 displayed parent structure of thiazole-substituted pyrazolones. Thirty-three such novel inhibitors of VEGFR-2 were taken from literature [20] with their biological activities in terms of $IC_{50}$ values ($IC_{50}$ values, i.e., the concentration (μM) of inhibitor that produces 50% inhibition of VEGFR-2) accordingly the $pIC_{50}$ ($-\log IC_{50}$) reported in Table 1. The data set divided into a training set of 23 molecules and test set of 10 molecules. Ligand-based and receptor-guided 3D-QSAR models were developed using pharmacophore identification and molecular docking method, respectively.

### 2.2. Generation of the common pharmacophore hypothesis (CPH)

The common pharmacophore hypotheses (CPH) were generated using PHASE [16]. Conformers were generated using MCMM/LMOD with OPLS-2005 force field [21]. The most dominating features, hydrogen bond acceptor (A), hydrogen bond donor (D), hydrophobic group (H), negatively charged group (N), positively charged group (P), and aromatic ring (R), were defined by a set of chemical structural patterns. Pharmacophore matching tolerance was 1 Å. Those CPHs considered, which indicated at least five sites common to all 33 molecules. Further, the best CPH was selected because of survival score.

**Table 1**
The molecular structure and observed activities [21] of pyrazolones.

| No. | $R_1$ | $R_2$ | $R_3$ | $R_4$ | $R_5$ | $IC_{50}$ (nM) | $pIC_{50}$ |
|---|---|---|---|---|---|---|---|
| 1 | $CH_3$ | H | H | H | H | 1000 | −3.00 |
| 2 | $CH_3$ | H | $CH_3$ | H | H | 95 | −1.98 |
| 3 | $CH_3$ | 5-F | $CH_3$ | H | H | 99 | −2.00 |
| 4 | $CH_3$ | 5-Cl | $CH_3$ | H | H | 152 | −2.18 |
| 5 | $CH_3$ | 5-Cl | H | H | H | 300 | −2.48 |
| 6 | $CH_3$ | 5-$OCH_3$ | $CH_3$ | H | H | 90 | −1.95 |
| 7 | $CH_3$ | 5-CN | $CH_3$ | H | H | 300 | −2.48 |
| 8 | $CH_3$ | 4-F | $CH_3$ | H | H | 137 | −2.14 |
| 9 | $CH_3$ | 4-Cl | $CH_3$ | H | H | 45 | −1.65 |
| 10 | $CH_3$ | 4-Br | $CH_3$ | H | H | 34 | −1.53 |
| 11 | $CH_3$ | 4-$OCH_3$ | $CH_3$ | H | H | 19 | −1.28 |
| 12 | $CH_3$ | 4-$OC2H_5$ | $CH_3$ | H | H | 38 | −1.58 |
| 13 | $CH_3$ | 4-$CH_3$ | $CH_3$ | H | H | 58 | −1.76 |
| 14 | $CH_3$ | 4-Br,5-$OCH_3$ | $CH_3$ | H | H | 23 | −1.36 |
| 15 | $CH_3$ | 7-$OCH_3$ | $CH_3$ | H | H | 109 | −2.04 |
| 16 | $CH_3$ | 4,7-bis-$OCH_3$ | $CH_3$ | H | H | 20 | −1.30 |
| 17 | H | 5-F | $CH_3$ | H | H | 48 | −1.68 |
| 18 | H | 5-Cl | $CH_3$ | H | H | 34 | −1.53 |
| 19 | H | 5-CN | $CH_3$ | H | H | 174 | −2.24 |
| 20 | H | 5-$COOCH_3$ | $CH_3$ | H | H | 73 | −1.86 |
| 21 | H | 5-$OCH_3$ | $CH_3$ | H | H | 28 | −1.45 |
| 22 | H | 5-Br | $CH_3$ | H | H | 110 | −2.04 |
| 23 | H | 5-$CH_3$ | $CH_3$ | H | H | 35 | −1.54 |
| 24 | H | 4-F | $CH_3$ | H | H | 16 | −1.20 |
| 25 | H | 4-Cl | $CH_3$ | H | H | 16 | −1.20 |
| 26 | H | 4-Br | $CH_3$ | H | H | 8 | −0.90 |
| 27 | H | 4-$OCH_3$ | $CH_3$ | H | H | 13 | −1.11 |
| 28 | H | 4-$OC_2H_5$ | $CH_3$ | H | H | 25 | −1.40 |
| 29 | H | 4-$COOCH_3$ | $CH_3$ | H | H | 22 | −1.34 |
| 30 | H | 4-Br, 5-$OCH_3$ | $CH_3$ | H | H | 6 | −0.78 |
| 31 | H | 6-Cl | $CH_3$ | H | H | 73 | −1.86 |
| 32 | H | 4-Br, 6-$CH_3$ | $CH_3$ | H | H | 12 | −1.08 |
| 33 | H | 4,7-bis-$OCH_3$ | $CH_3$ | H | H | 10 | −1.00 |

### 2.3. Assessment of significant CPHs using partial least square (PLS) analyses

The evaluation of generated CPHs performed by correlating the observed and estimated activity for the training set of 23 molecules and test set of 10 molecules. Partial least square (PLS) analyses performed using strike with maximum N/3 PLS factors, N1/3 number of ligands in training set, and either atom, or pharmacophore-based model using grid spacing of 1 Å. CPHs of significant statistical values were selected for molecular alignments to use in ligand-based CoMFA and CoMSIA.

### 2.4. Molecular docking

The crystal structure of VEGFR-2 (PDB = 1YWN) was used as receptor for molecular docking studies. The inhibitor structure was minimized using OPLS-2005 [21] force field in Macro Model. The molecular docking performed using GLIDE docking tool with standard protocols. The active site was defined within 5Å surrounding to the co-crystallized ligand and the specific residues and constraints information were obtained from crystallographic data as well as an earlier study [20]. The final ligand binding poses were ranked according to a computed model score that encompasses the grid score, proprietary GLIDE score, and the internal energy strain. The inhibitors were docked in to the receptor site using GLIDE docking algorithm in the SP (standard precision) mode. Docked geometry based alignment was used for receptor-guided CoMFA and CoMSIA.

### 2.5. 3D-QSAR

The 3D-QSAR models were developed using CoMFA and CoMSIA techniques.

### 2.6. CoMFA and CoMSIA

The initial setup for CoMFA and CoMSIA was similar to our earlier work [10,22,23]. In summary CoMFA were studied using steric and electrostatic potential fields while CoMSIA was based on five different properties (steric, electrostatic, hydrophobic, H-bond donors and acceptors). All the calculations were performed using Sybyl software [24].

### 2.7. Partial least square (PLS) analysis and validation of QSAR models

To derive 3D-QSAR models, the CoMFA and CoMSIA descriptors were used as independent variables and the $pIC_{50}$ values as dependent variable. PLS method [25,26] was used to linearly correlate these CoMFA and CoMSIA descriptors to the activity. The basic statistical setup was same as defined in our earlier works [10,22,27]. To have robustness and statistical confidence of the derived models, bootstrapping analysis used for 10 runs. To assess the predictive power of the derived 3D-QSAR models, activity of test set of 10 molecules were predicted. The predictive abilities of the models expressed by the predictive $r^2$ value, which is analogous to cross-validated $r^2(q^2)$.

**Table 2**
The regression summary of pharmacophore-based QSAR models.

| No. | Analyses | $n$ | $q^2$ | $r^2$ | SD | RMSE | $F$ | $R$ |
|---|---|---|---|---|---|---|---|---|
| $PA_1$ | CHPs score | 1 | 0.28 | 0.45 | 0.4 | 0.37 | 16.9 | – |
| $PA_2$ | CHPs score | 2 | 0.22 | 0.56 | 0.36 | 0.38 | 12.8 | – |
| $PA_3$ | CHPs score | 3 | 0.32 | 0.62 | 0.35 | 0.36 | 10.4 | – |
| $PA_4$ | CHPs score | 4 | 0.5 | 0.73 | 0.3 | 0.31 | 12 | – |
| $PA_5$ | CHPs score | 1 | 0.28 | 0.44 | 0.4 | 0.37 | 16.9 | – |
| $PA_6$ | CHPs score | 2 | 0.22 | 0.56 | 0.36 | 0.38 | 12.8 | – |
| $PA_7$ | CHPs score | 3 | 0.32 | 0.62 | 0.35 | 0.36 | 10.4 | – |
| $PA_8$ | CHPs score | 4 | 0.5 | 0.73 | 0.3 | 0.31 | 12 | – |
| $PA_9$ | CHPs score | 1 | 0.35 | 0.53 | 0.36 | 0.35 | 24.1 | – |
| $PA_{10}$ | CHPs score | 2 | 0.41 | 0.64 | 0.33 | 0.34 | 17.6 | – |
| $PA_{11}$ | CHPs score | 3 | 0.46 | 0.69 | 0.31 | 0.32 | 13.8 | – |
| $PA_{12}$ | CHPs score | 4 | 0.54 | 0.81 | 0.25 | 0.3 | 18.6 | 0.75 |

## 3. Results

### 3.1. Pharmacophore

The training set used to identify the CPH by using tree based partition algorithms. Based on sites, hydrophobic (H), negative (N) and ring (R) maximum five features were allowed to develop hypothesis and a number of CPHs were reported common in all 33 molecules. There were six hypotheses based on combination ADHRR, 20 hypotheses based on AAADR, 3 hypotheses based on AAHRR, 42 hypotheses based on AADRR, 3 hypotheses based on AADHR, 11 hypotheses based on AAARR, 4 hypotheses based on AARRR and 10 hypotheses based on ADRRR. Three hypotheses namely AADRR (survival score = 3.84), AADRR (survival score = 3.84) and AARRR (survival score = 3.83) were selected for molecular alignment. PLS analyses conducted using four factors with a grid spacing 0.5 Å. Twelve regression models were derived. The regression summary reported in Table 2. The best-fitted model-$PA_{12}$ ($q^2 = 0.54$, $r^2 = 0.81$, $F = 18.6$, $R_{testset} = 0.75$) used for activity prediction of training and test sets as reported in Table 4.

The selected pharmacophores were displayed in Figs. 2 and 4. The red ball showed hydrogen bond acceptor site while the brown ring demonstrates the R (ring) pharmacophore. In Fig. 2, binding mode as reported in crystal data and pharmacophore distributions within active site were displayed. The both ligands are different but having same scaffold. The green stick displaying co-crystallized ligand while the grey sticks for template of pharmacophore-based model. Both the ligands have good overlap and the hydrogen bond acceptor sites of pyrazlone ring, directed towards hinge region that facilitate hydrogen bonding with receptor. Such hydrogen bonds are key interaction in kinases. The pharmacopore perception inside the receptor active site gives an insight to the selection of these features as pharmacophore.

### 3.2. Molecular docking and scoring function based QSAR

All the molecules were docked in to the receptor site using GLIDE docking tool with standard protocols. The initial protein coordinates used in this study are those reported in the X-ray crystal structure (1YWN). During grid generation the H bond to Cys917, position of oxygen and hydrophobic zone were used as constraints. The binding mode of inhibitor-30 in the active site of VEGFR-2 is shown in Fig. 3. As we can see from Fig. 3 the lactam ring of the pyrazolone has one hydrogen donor NH connected with GLU-915 and one carbonyl oxygen bound to the Cys-917 and the thiadiazole ring near the salt bridge Lys-866. This binding mode is quite similar to the binding mode proposed earlier [20].

### 3.3. 3D-QSAR

The CoMFA and CoMSIA require 3D aligned structures according to suitable conformational template [28]. In the present study the ligand-based and receptor-guided two different molecular alignments were used.

### 3.4. Alignment method-1

In a ligand-based technique, molecules were aligned on template, using best fitted and statistically significant CPHs (AARRR)-based model-12 as shown in Fig. 4 and subsequently used for CoMFA/CoMSIA probe interaction energy calculations.

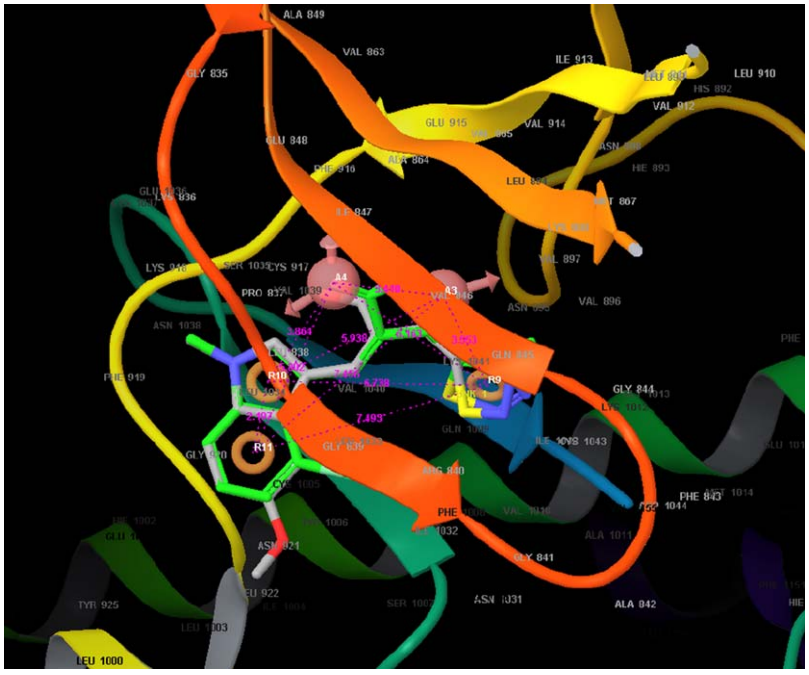


**Fig. 2.** Perception of the common pharmacophores within the active site. The green stick displaying co-crystallized ligand while the grey sticks for dock ligand (acceptor = pink ball, aromatics rings = brown ring).

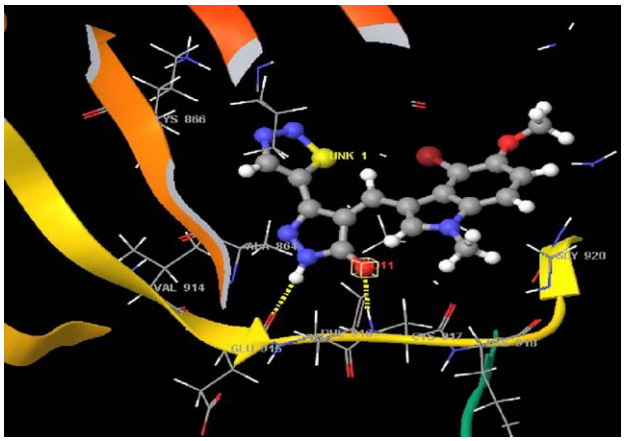


**Fig. 3.** Docked pose of the most active molecule (compound-30) within active site.

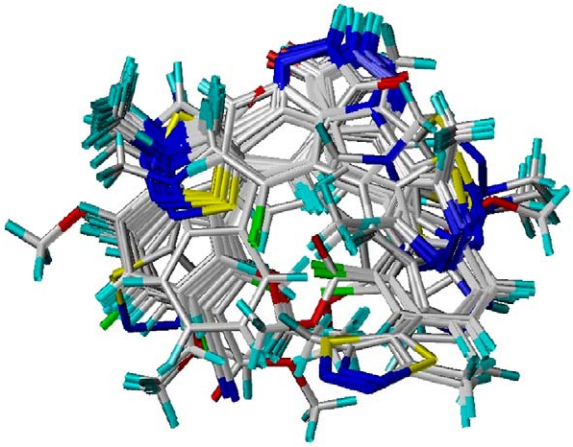

**Fig. 5.** The molecular alignment based on method-2.

### 3.5. Alignment method-2

The receptor-guided technique was used. The best-docked geometries of molecules were obtained from GLIDE pose viewer. The selection criteria involved docking-based scores and more importantly, the knowledge-based pose selection. The only those conformer of all molecules were selected, which have binding mode very close to co-crystal structure. Each molecule acquires its preferential site in receptor active site. The best fitted conformer of all the molecules were extracted as shown in Fig. 5. This molecular alignment is more realistic and more suitable for molecular field analyses. The same alignment was subsequently used for CoMFA–CoMSIA interaction energy calculations.

### 3.6. Comparative molecular field analysis (CoMFA)

CoMFA models were developed using geometrical scheme-1 (statistically significant CPH-based alignment = AARRR). The aligned molecular geometries were used in Sybyl and charges were assigned with the Gasteiger–Hückel method [29]. Previously defined training and test sets were used to correlate the biological activities against CoMFA fields. Three different CoMFA models ($PA_{13}$–$PA_{15}$) were derived utilizing steric "S", electrostatic "E" and jointly both fields. The regression summary reported in Table 3. The model $PA_{15}$ based on both steric and electrostatic field was most successful as clear from statistics, the cross-validated leave on out $q^2 = 0.70$ with five components, non cross-validated $r^2 = 0.97$ with SEE = 0.09 and $F = 121.6$. The success of model was tested for internal predictivity ($r^2_{\text{boot strapping}} = 0.99$, SD = 0.001) and test set predictivity of 10 molecules ($r^2_{\text{predictive}} = 0.61$). The predicted activities by model $PA_{15}$ were reported in Table 4. Similarly, the CoMFA was performed using geometrical scheme-2 (docked geometry). The docked geometries of all molecules were imported in Sybyl and charges were assigned with the Gasteiger–Hückel method. The same training and test sets used to correlate the biological activities against CoMFA. Three

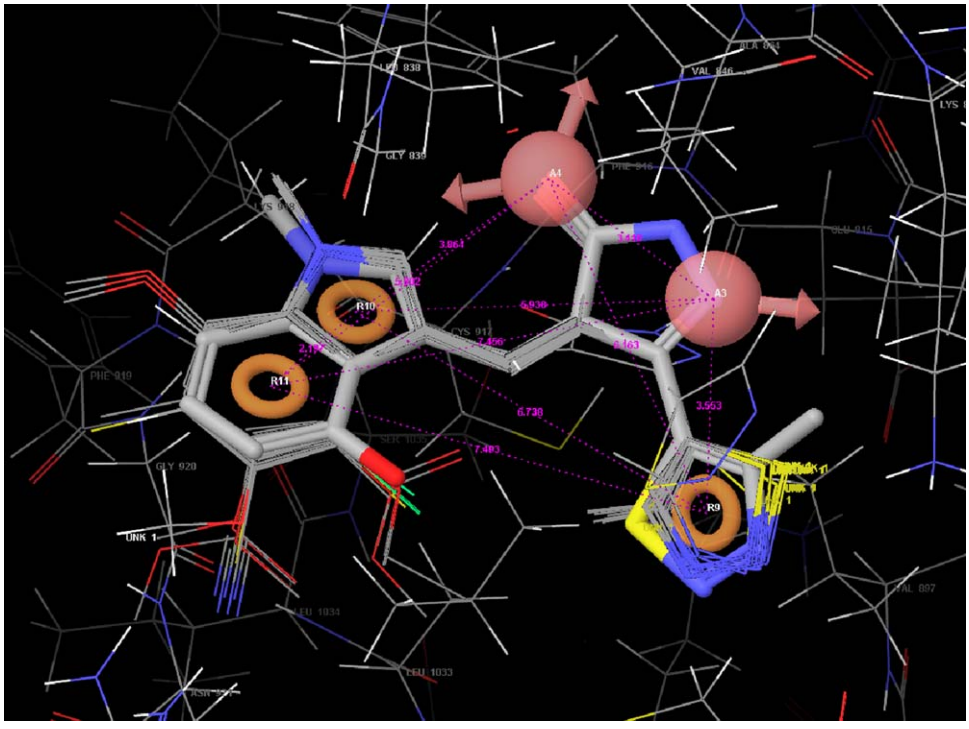


**Fig. 4.** The molecular alignment based on method-1. Aligned ligands and common pharmacophores within the active site (acceptor = pink ball, aromatics rings = brown ring).

**Table 3**
The regression summary of different CoMFA and CoMSIA based models.

| No. | Analyses | Geometry | Field | $n$ | $q^2$ | $r^2$ | $F$ | SE | $r^2_{\text{boot strapping}}$ | SD | $r^2_{\text{predictive}}$ |
|---|---|---|---|---|---|---|---|---|---|---|---|
| $PA_{13}$ | CoMFA | CPHs | S | 5 | 0.67 | – | – | – | – | – | – |
| $PA_{14}$ | CoMFA | CPHs | E | 5 | 0.55 | – | – | – | – | – | – |
| $PA_{15}$ | CoMFA | CPHs | 0.78S/0.22E | 5 | 0.7 | 0.97 | 121.6 | 0.09 | 0.99 | 0.01 | 0.61 |
| $PA_{16}$ | CoMFA | Docked | S | 5 | 0.46 | – | – | – | – | – | – |
| $PA_{17}$ | CoMFA | Docked | E | 3 | 0.28 | – | – | – | – | – | – |
| $PA_{18}$ | CoMFA | Docked | 0.64S/0.36E | 5 | 0.56 | 0.97 | 108.9 | 0.1 | 0.98 | 0.01 | 0.82 |
| $PA_{19}$ | CoMSIA | CPHs | S | 5 | 0.33 | – | – | – | – | – | – |
| $PA_{20}$ | CoMSIA | CPHs | E | 3 | 0.50 | – | – | – | – | – | – |
| $PA_{21}$ | CoMSIA | CPHs | H | 4 | 0.53 | – | – | – | – | – | – |
| $PA_{22}$ | CoMSIA | CPHs | D | 1 | −.01 | – | – | – | – | – | – |
| $PA_{23}$ | CoMSIA | CPHs | A | 3 | −23 | – | – | – | – | – | – |
| $PA_{24}$ | CoMSIA | CPHs | 0.54S/0.46E | 5 | 0.49 | – | – | – | – | – | – |
| $PA_{25}$ | CoMSIA | CPHs | 0.39S/0.31E/0.30H | 2 | 0.54 | 0.82 | 44.98 | 0.23 | 0.81 | 0.05 | 0.66 |
| $PA_{25}$ | CoMSIA | CPHs | 0.17S/0.19E/0.64A | 4 | 0.31 | – | – | – | – | – | – |
| $PA_{27}$ | CoMSIA | Docked | S | 5 | 0.21 | – | – | – | – | – | – |
| $PA_{28}$ | CoMSIA | Docked | E | 2 | 0.22 | – | – | – | – | – | – |
| $PA_{329}$ | CoMSIA | Docked | H | 1 | 0.07 | – | – | – | – | – | – |
| $PA_{30}$ | CoMSIA | Docked | D | 4 | −0.2 | – | – | – | – | – | – |
| $PA_{31}$ | CoMSIA | Docked | A | 1 | −0.17 | – | – | – | – | – | – |
| $PA_{32}$ | CoMSIA | Docked | 0.45S/0.55E | 2 | 0.16 | – | – | – | – | – | – |
| $PA_{33}$ | CoMSIA | Docked | 0.33S/0.27E/0.40H | 3 | 0.21 | – | – | – | – | – | – |
| $PA_{34}$ | CoMSIA | Docked | 0.26S/0.25E/0.25A | 5 | 0.58 | 0.91 | 36.3 | 0.17 | 0.96 | 0.02 | 0.69 |

different models ($PA_{16}$–$PA_{18}$) based on steric "S", electrostatic "E" and jointly both fields were developed. The regression summary reported in Table 3. The model $PA_{18}$ based on joint field effects was successful as clear from statistics, the cross-validated leave on out $q^2 = 0.56$ with five components, non-cross validated $r^2 = 0.97$ with SEE = 0.08 and $F = 108.9$. The success of model was tested for internal predictivity ($r^2_{\text{boot strapping}} = 0.98$, SD = 0.01) and test set predictivity of 10 molecules ($r^2_{\text{predictive}} = 0.82$). The receptor-guided CoMFA has overall best statistics and high predictivity. Since this analysis was based on automated pharmacophore distribution under the influence of receptor site, hence it seems more realistic and meaningful. The predicted activities of test and training sets

**Table 4**
The observed [21] and predicted activities using 3D-QSAR models.

| No. | $pIC_{50}$ | CPHs | | CPHs | | CPHs | | Docked | | Docked | |
|---|---|---|---|---|---|---|---|---|---|---|---|
| | | $PA_{12}$ | Residues | $PA_{15}$ | Residues | $PA_{25}$ | Residues | $PA_{18}$ | Residues | $PA_{34}$ | Residues |
| 1 | 3 | 2.96 | 0.04 | 2.977 | 0.023 | 2.491 | 0.509 | 2.951 | 0.049 | 3.15 | −0.15 |
| 2 | 1.97 | 2.15 | −0.18 | 2.04 | −0.07 | 2.245 | −0.275 | 2.006 | −0.036 | 2.052 | −0.082 |
| 3 | 1.99 | 1.78 | 0.21 | 2.121 | −0.131 | 2.244 | −0.254 | 2.162 | −0.172 | 1.824 | 0.166 |
| 6 | 1.95 | 2.04 | −0.09 | 1.927 | 0.023 | 2.108 | −0.158 | 1.936 | 0.014 | 1.776 | 0.174 |
| 7 | 2.47 | 2.45 | 0.02 | 2.516 | −0.046 | 2.376 | 0.094 | 2.457 | 0.013 | 2.427 | 0.043 |
| 9 | 1.65 | 1.6 | 0.05 | 1.614 | 0.036 | 1.761 | −0.111 | 1.6 | 0.05 | 1.578 | 0.072 |
| 10 | 1.53 | 1.76 | −0.23 | 1.506 | 0.024 | 1.303 | 0.227 | 1.574 | −0.044 | 1.619 | −0.089 |
| 12 | 1.57 | 1.65 | −0.08 | 1.501 | 0.069 | 1.437 | 0.133 | 1.577 | −0.007 | 1.508 | 0.062 |
| 13 | 1.76 | 1.59 | 0.17 | 1.606 | 0.154 | 1.723 | 0.037 | 1.883 | −0.123 | 1.793 | −0.033 |
| 14 | 1.36 | 1.52 | −0.16 | 1.401 | −0.041 | 1.242 | 0.118 | 1.172 | 0.188 | 1.451 | −0.091 |
| 15 | 2.03 | 1.62 | 0.41 | 1.961 | 0.069 | 2.017 | 0.013 | 1.99 | 0.04 | 1.688 | 0.342 |
| 16 | 1.3 | 1.36 | −0.06 | 1.365 | −0.065 | 1.474 | −0.174 | 1.371 | −0.071 | 1.254 | 0.046 |
| 18 | 1.53 | 1.52 | 0.01 | 1.668 | −0.138 | 1.767 | −0.237 | 1.616 | −0.086 | 1.715 | −0.185 |
| 19 | 2.24 | 1.97 | 0.27 | 2.15 | 0.09 | 1.95 | 0.29 | 2.126 | 0.114 | 2.185 | 0.055 |
| 21 | 1.44 | 1.71 | −0.27 | 1.456 | −0.016 | 1.472 | −0.032 | 1.39 | 0.05 | 1.57 | −0.13 |
| 23 | 1.54 | 1.55 | −0.01 | 1.465 | 0.075 | 1.527 | 0.013 | 1.447 | 0.093 | 1.429 | 0.111 |
| 25 | 1.2 | 1.1 | 0.1 | 1.006 | 0.194 | 1.316 | −0.116 | 1.222 | −0.022 | 1.141 | 0.059 |
| 26 | 0.9 | 1.12 | −0.22 | 1.041 | −0.141 | 1.149 | −0.249 | 0.882 | 0.018 | 0.991 | −0.091 |
| 28 | 1.39 | 1.24 | 0.15 | 1.431 | −0.041 | 1.039 | 0.351 | 1.253 | 0.137 | 1.288 | 0.102 |
| 29 | 1.34 | 1.43 | −0.09 | 1.311 | 0.029 | 1.531 | −0.191 | 1.345 | −0.005 | 1.252 | 0.088 |
| 30 | 0.77 | 1.07 | −0.3 | 0.822 | −0.052 | 0.814 | −0.044 | 0.96 | −0.19 | 1.197 | −0.427 |
| 32 | 1.07 | 0.82 | 0.25 | 1.076 | −0.006 | 0.933 | 0.137 | 1.083 | −0.013 | 1.128 | −0.058 |
| 33 | 1 | 0.98 | 0.02 | 1.042 | −0.042 | 1.082 | −0.082 | 0.998 | 0.002 | 0.985 | 0.015 |
| Test set | | | | | | | | | | | |
| 4 | 2.18 | 2.1 | 0.08 | 2.021 | 0.159 | 2.188 | −0.008 | 2.022 | 0.158 | 1.89 | 0.29 |
| 5 | 2.47 | 2.57 | −0.1 | 2.958 | −0.488 | 2.435 | 0.035 | 2.318 | 0.152 | 3.097 | −0.627 |
| 8 | 2.13 | 1.68 | 0.45 | 1.897 | 0.233 | 1.917 | 0.213 | 1.496 | 0.634 | 1.595 | 0.535 |
| 11 | 1.27 | 1.73 | −0.46 | 1.512 | −0.242 | 1.807 | −0.537 | 1.529 | −0.259 | 1.512 | −0.242 |
| 17 | 1.69 | 1.43 | 0.26 | 1.774 | −0.084 | 1.828 | −0.138 | 1.69 | 0 | 1.711 | −0.021 |
| 20 | 1.86 | 1.7 | 0.16 | 1.586 | 0.274 | 1.577 | 0.283 | 1.765 | 0.095 | 2.388 | −0.528 |
| 22 | 2.04 | 1.55 | 0.49 | 1.618 | 0.422 | 1.748 | 0.292 | 1.622 | 0.418 | 1.726 | 0.314 |
| 24 | 1.2 | 1.03 | 0.17 | 1.542 | −0.342 | 1.499 | −0.299 | 1.217 | −0.017 | 1.362 | −0.162 |
| 27 | 1.11 | 1.3 | −0.19 | 1.17 | −0.06 | 1.389 | −0.279 | 1.318 | −0.208 | 1.308 | −0.198 |
| 31 | 1.86 | 1.13 | 0.73 | 1.662 | 0.198 | 1.831 | 0.029 | 1.754 | 0.106 | 1.71 | 0.15 |

The negative values of all activities were converted in to positive by multiplying −1.

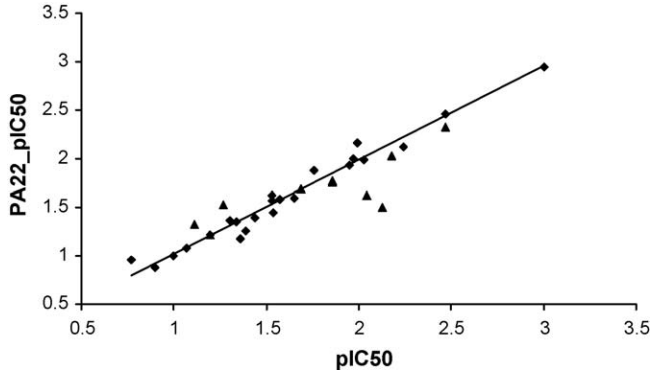


**Fig. 6.** Trend of observed and predicted $pIC_{50}$ values using geometrical scheme-2-based CoMFA model ($PA_{18}$).

were reported in Table 4 and the trend of observed and predicted activities of training and test sets by model $PA_{18}$ is shown in Fig. 6.

### 3.7. CoMFA contour maps

Fig. 5 showed CoMFA steric map within the active site of receptor. CoMFA model $PA_{18}$ used to draw the map with most active ligand. Sterically favored areas represented by green polyhedron and disfavored areas are represented by yellow polyhedron. The CoMFA steric map encompasses green contours around position C-4, C-5 and $R_3$ indicated that, steric bulk might increase the activity. It is clear from molecular docking the position C-4 and $R_3$ correspond to hydrophobic zone of receptor site showed by brown color of MOLCAD surface (Fig. 7). Similarly, the position C-5 directed towards a hallow pocket and bulkiness around this position may facilitate the contact and might be helpful to improve the activity.Fig. 8 showed CoMFA electrostatic contour map within the active site of receptor. The positive charge favored areas represented by blue polyhedron and negative charge favored areas by red polyhedron. As we can see, the blue contour appears near to methoxy group of position-5. The methoxy group directed towards negative zone of receptor site and positive substituents around methoxy group may facilitate the binding. The nitrogen adjacent to site $R_1$ holds a red contour and a negative group around this region might be helpful to improve the activity.

The CoMSIA models were made using five field descriptors namely (steric, electrostatic, hydrophobic, hydrogen bond donor and acceptor) with same molecular alignment as for CoMFA. In case of geometrical scheme-1, the steric, electrostatic and hydrophobic fields individually showed good relationship and the combination of all these three fields (model $PA_{25}$) gave significant result ($q^2 = 0.54$, $r^2 = 0.82$). The model $PA_{25}$ showed good external predictivity ($r^2_{predictive} = 0.66$) for 10 molecules of test set. The geometrical scheme-2 also used to derive CoMSIA, the combination of steric, electrostatic and hydrogen bond acceptor fields (model $PA_{34}$) gave significant result ($q^2 = 0.58$, $r^2 = 0.91$) with external predictivity ($r^2_{predictive} = 0.69$) for test set. The statistics of geometrical scheme-2 based model $PA_{34}$ was better than geometrical scheme-1. The regression results of different CoMSIA models are reported in Table 4 and the predicted activities by CoMSIA model $PA_{25}$ and $PA_{34}$ are reported in Table 4. The trends model $PA_{34}$-based predicted and observed activities of training and test sets, is displayed in Fig. 9.

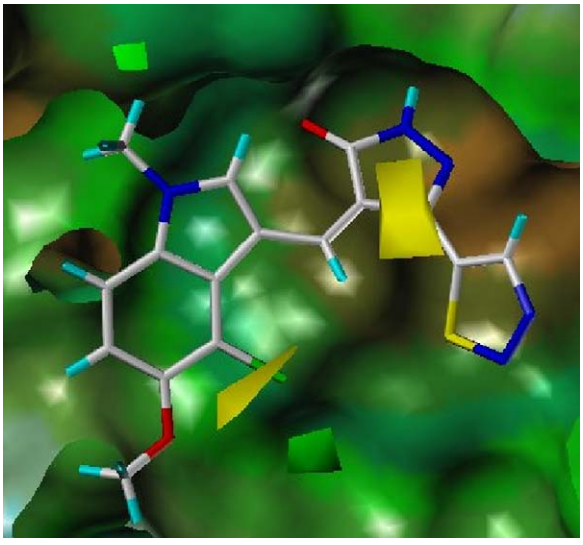

**Fig. 7.** The model $PA_{18}$ (alignment method-2)-based CoMFA steric contour map.

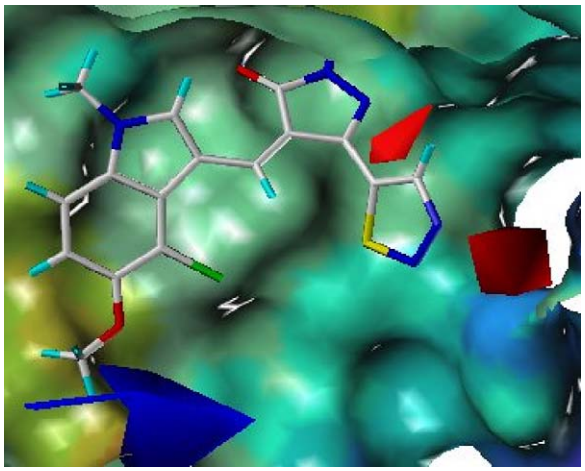

**Fig. 8.** The model $PA_{18}$ (alignment method-2)-based CoMFA electrostatic contour map. Comparative molecular similarity indices analysis (CoMSIA).

### 3.8. CoMSIA contour maps

The model $PA_{34}$-based CoMSIA steric contour map developed and displayed in Fig. 10 with template (ligand-30). The map is quite similar to CoMFA map and holds a green contour around site C-5 while yellow contour around sulfur atom. It is clear from map the binding pocket is hydrophobic in nature and the site 5 significantly corresponds to hallow pocket. A bulky group around

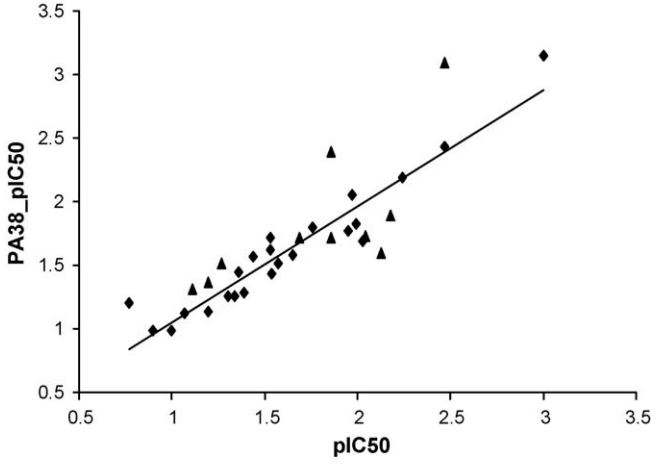


**Fig. 9.** Trend of observed and predicted pIC50 values using geometrical scheme-2-based CoMSIA model ($PA_{34}$).

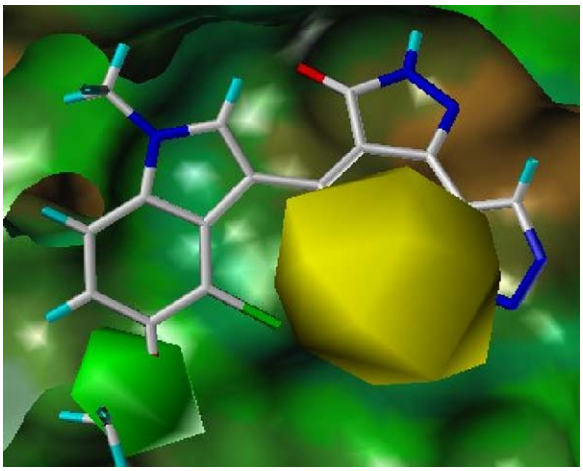

**Fig. 10.** The model $PA_{34}$ (alignment method-2)-based CoMSIA steric contour map.

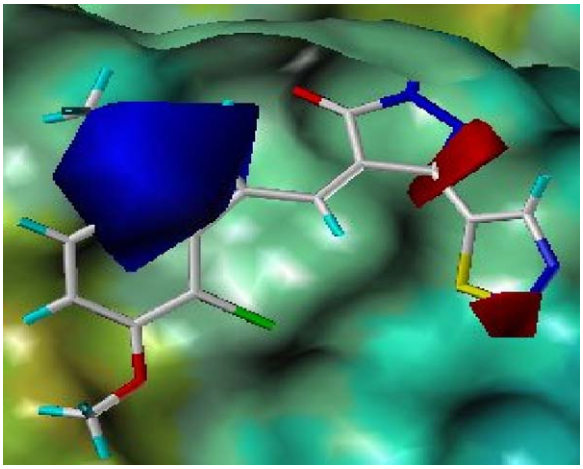

**Fig. 11.** The model $PA_{34}$ (alignment method-2)-based CoMSIA electrostatic contour map.

these two positions might be favorable but a small group is desirable near to sulfur.

Similarly, Fig. 11 shows CoMSIA electrostatic contour map and a small red contour appears around pyrrzolone and thiadiazole rings, which indicated that a negative group around these sites might be helpful to improve the activity. A blue contour appears near to pyrrole moiety, since the surrounding is negative in nature so a positive group is desirable to improve the activity.

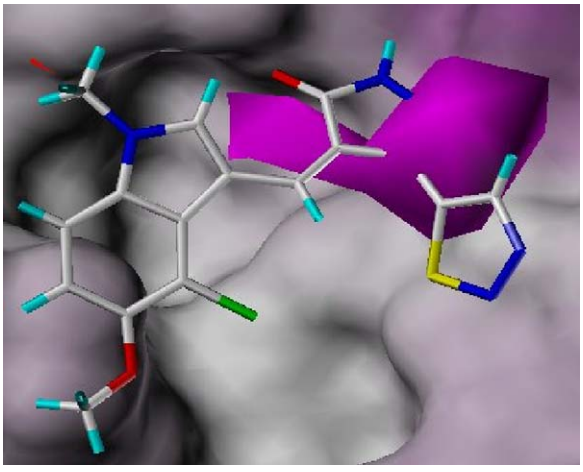

**Fig. 12.** The model $PA_{34}$ (alignment method-2)-based CoMSIA hydrogen bond acceptor contour map.

Since the model, $PA_{34}$ was based on steric, electrostatic and hydrogen bond acceptor fields effects. The hydrogen bond acceptor map was drawn and displayed in Fig. 12. Magenta contour appears around pyrazolones moiety indicated that a hydrogen bond acceptor group is desirable around this region. It is clear from molecular docking this region of inhibitor is located towards hinge region of receptor and holds two hydrogen bonds with residue 915 and 916 as clear from Fig. 3, reasonably some hydrogen bond acceptor group might be helpful to improve the activity.

## 4. Discussion

The main aim of this study was to establish a prominent relationship between structural features with inhibitory activity. A consistency between results and agreement with earlier studies were noticed and discussed. Here we have derived QSAR models using different methods based on two prominent (ligand-based and receptor-guided) techniques. In a recent study, Tripathi et al. pointed out two hydrogen bonding site in pyrazlone ring and a hydrophobic zone due to aromatic group. In our pharmacophore mapping study these two sites of pyrazlone ring were found an important feature and it was consistent in whole series. The pharmacophore-based study ($q^2 = 0.54$, $r^2 = 0.81$ and $R = 0.75$) indicated a possible steric hydrophobic and hydrogen bond acceptor interaction of ligand to VEGFR-2. The statistical value it self is not very high but more importantly the identified features are common in whole series and the insights are further supported by receptor-guided techniques. This best-fitted model was used to develop ligand-based CoMFA and CoMSIA. The ligand-based CoMFA model $PA_{15}$ gave good result ($q^2 = 0.7$, $r^2 = 0.97$, $r^2_{\text{predictive}} = 0.61$) in which the steric field contribution was 78% while electrostatic field contribution was 22%. Similarly ligand-based CoMSIA model $PA_{25}$ gave good result ($q^2 = 0.54$, $r^2 = 0.82$, $r^2_{\text{predictive}} = 0.66$) in which the contributions of steric, electrostatic and hydrophobic fields were 39%, 31% and 30%, respectively. In this way, the pharmacophores-based study implies strong steric and electrostatic interactions. CoMSIA has special interest, as there was hydrophobic interaction but no hydrogen bonding interaction. This is probably due to dominance of hydrophobic (aromatic) interaction over hydrogen bonding as reflected from statistics reported in Table 3.

The pharmacophore identification gives an idea about possible interaction, as it looks to common features along the series. The main drawback of ligand-based pharmacophore identification is the lack of receptor structure. The groups in ligands are not able to locate their counterpart (receptor site) in space. The pharmacophore-based alignment forces to allocate all similar groups together while in reality the complex receptor exists. The ligands will adjust their geometries because of interaction with the receptor. Thus, regarding receptor structure pharmacophore model generation will be more meaningful and helpful to identify the local interactions between ligand sites and their counter parts in the receptor.

Consequently, we employed molecular docking. All the molecules were docked and their top score poses were identified. In molecular docking, the molecules acquire their preferential sites in to receptor protein. The molecules acquires almost same sites as reported in earlier study [20] and they all have significant interaction with residues 915 and 916. The pyrazlone ring directed towards hinge region, particularly to residue 915–916 where it makes important hydrogen bonding as clear from Figs. 2 and 3.

The CoMFA and CoMSIA were developed using molecular docking-based on automated molecular alignment. The receptor-

guided CoMFA model $PA_{18}$ gave good results ($q^2$ = 0.56, $r^2$ = 0.97, $r^2_{predictive} = 0.82$). In this model, the steric and electrostatic contributions were 64% and 36%, respectively. The receptor-guided CoMSIA model $PA_{34}$ gave significant results ($q^2$ = 0.58 $r^2$ = 0.91, $r^2_{predictive} = 0.69$) also indicated a combine interaction of steric, electrostatic and hydrogen bond acceptor field effects. The receptor-guided CoMSIA was in agreement with pharmacophores-based model, the overall study indicated, the steric, electrostatic, and hydrogen bond acceptor interactions are involved in to the interaction with KDR.

The receptor-guided alignment generally gives meaningful statistics, because the activity data is originated from the ligand–receptor interactions. Even If we have used a wrong binding pose, the statistics obtained from pharmacophore alignment could be better. Therefore, the statistically less significant pharmacophore models might signify correct binding pose while a statistically significant pharmacophore models might have poor binding pose. Thus, a model derived from combined approach incorporated both techniques would be significant.

## 5. Conclusion

In our study, we have built a pharmacophore model applying ligand-based pharmacophore generation approach, using PHASE. The resulting best hypothesis consisted of five features: two hydrogen bond acceptor and three-ring aromatic function. The pharmacophore-based study indicates a possible steric, hydrophobic and hydrogen bond acceptor interactions of ligands to VEGFR-2. The pharmacophore-based CoMFA and CoMSIA results were indicated a combine interaction of steric, electrostatic, and hydrophobic field effects. In receptor-guided study, we employed molecular docking and the docking-based alignment used for CoMFA/CoMSIA. The receptor-guided CoMFA and CoMSIA showed a combine interaction of steric, electrostatic and hydrogen bond acceptor effects. A positive bulkiness with hydrophobic effect could be desirable around positions 4 and 5. The hydrogen bond acceptor groups around carbonyl oxygen and nitrogen of pyrazolones moiety may facilitate the binding with hinge region and might be helpful to improve the activity.

## Acknowledgments

We are thankful to Dr. Aline Thomas, IBS Grenoble France for valuable suggestions and Mr. Hwan Won Chung for help.

## References

[1] M. Hasegawa, N. Nishigaki, Y. Washio, K. Kano, P.A. Harris, H. Sato, I. Mori, R.I. West, M. Shibahara, H. Toyoda, L. Wang, R.T. Nolte, J.M. Veal, M. Cheung, J. Med. Chem. 50 (18) (2007) 4453–4470.
[2] L.B. Jakeman, M. Armanini, H.S. Phillips, N. Ferrara, Endocrinology 133 (2) (1993) 848–859.
[3] C. de Vries, J.A. Escobedo, H. Ueno, K. Houck, N. Ferrara, L.T. Williams, Science 255 (5047) (1992) 989–991.
[4] B.I. Terman, M. Dougher-Vermazen, M.E. Carrion, D. Dimitrov, D.C. Armellino, D. Gospodarowicz, P. Bohlen, Biochem. Biophys. Res. Commun. 187 (3) (1992) 1579–1586.
[5] M. Klagsbrun, M.A. Moses, Chem. Biol. 6 (8) (1999) R217–R224.
[6] L.M. Strawn, G. McMahon, H. App, R. Schreck, W.R. Kuchler, M.P. Longhi, T.H. Hui, C. Tang, A. Levitzki, A. Gazit, I. Chen, G. Keri, L. Orfi, W. Risau, I. Flamme, A. Ullrich, K.P. Hirth, L.K. Shawver, Cancer Res. 56 (15) (1996) 3540–3545.
[7] Y.J. Dai, Y. Guo, R.R. Frey, Z.Q. Ji, M.L. Curtin, A.A. Ahmed, D.H. Albert, L. Arnold, S.S. Arries, T. Barlozzari, J.L. Bauch, J.J. Bouska, P.F. Bousquet, G.A. Cunha, K.B. Glaser, J. Guo, J.L. Li, P.A. Marcotte, K.C. Marsh, M.D. Moskey, L.J. Pease, K.D. Stewart, V.S. Stoll, P. Tapang, N. Wishart, S.K. Davidsen, M.R. Michaelides, J. Med. Chem. 48 (19) (2005) 6066–6083.
[8] R.M. Borzilleri, X. Zheng, L. Qian, C. Ellis, Z.W. Cai, B.S. Wautlet, S. Mortillo, R. Jeyaseelan Sr., D.W. Kukral, A. Fura, A. Kamath, V. Vyas, J.S. Tokarski, J.C. Barrish, J.T. Hunt, L.J. Lombardo, J. Fargnoli, R.S. Bhide, J. Med. Chem. 48 (12) (2005) 3991–4008.
[9] K. Paz, Z. Zhu, Front Biosci. 10 (2005) 1415–1439.
[10] F.A. Pasha, M. Muddassar, S.J. Cho, K. Ahmad, Y. Beg, Eur. J. Med. Chem. 43 (11) (2008) 2361–2372.
[11] F.A. Pasha, M. Muddassar, S.J. Cho, Y. Beg, K. Ahmad, Eur. J. Med. Chem. 43 (11) (2008) 23612372.
[12] F.A. Pasha, M.M. Neaz, S.J. Cho, S.B. Kang, Chem. Biol. Drug Des. 70 (6) (2007) 520–529.
[13] F.A. Pasha, H.K. Srivastava, P.P. Singh, Int. J. Quantum Chem. 104 (1) (2005) 87–100.
[14] F.A. Pasha, H.K. Srivastava, P.P. Singh, Bioorg. Med. Chem. 13 (24) (2005) 6823–6829.
[15] F.A. Pasha, H.K. Srivastava, A. Srivastava, P.P. Singh, QSAR Comb. Sci. 26 (1) (2007) 69–84.
[16] Phase, version 8.0 (2007).
[17] Y. Miyazaki, S. Matsunaga, J. Tang, Y. Maeda, M. Nakano, R.J. Philippe, M. Shibahara, W. Liu, H. Sato, L. Wang, R.T. Nolte, Bioorg. Med. Chem. Lett. 15 (9) (2005) 2203–2207.
[18] R.D. Cramer, D.E. Patterson, J.D. Bunce, J. Am. Chem. Soc. 110 (18) (1988) 5959–5967.
[19] G. Klebe, U. Abraham, T. Mietzner, J. Med. Chem. 37 (24) (1994) 4130–4146.
[20] R. Tripathy, A. Ghose, J. Singh, E.R. Bacon, T.S. Angeles, S.X. Yang, M.S. Albom, L.D. Aimone, J.L. Herman, J.P. Mallamo, Bioorg. Med. Chem. Lett. 17 (6) (2007) 1793–1798.
[21] G.A. Kaminski, R.A. Friesner, J. Tirado-Rives, W.L. Jorgensen, J. Phys. Chem. B 105 (28) (2001) 6474–6487.
[22] F.A. Pasha, M. Muddassar, S.J. Cho, Chem. Biol. Drug Des. 73 (3) (2009) 292–300.
[23] F.A. Pasha, M. Muddassar, Y. Beg, S.J. Cho, Chem. Biol. Drug Des. 71 (5) (2008) 483–493.
[24] SYBYL7.3; St. Louis, Missouri, USA.
[25] P. Geladi, Y.L. Xie, A. Polissar, P. Hopke, J. Chemom. 2 (1998) 231.
[26] S. Wold, A. Ruhe, H. Wold, W.J. Dunn, Siam J. Sci. Stat. Comput. 5 (3) (1984) 735–743.
[27] F.A. Pasha, H.W. Chung, S.B. Kang, S.J. Cho, Int. J. Quantum Chem. 108 (2) (2008) 391–400.
[28] K.H. Kim, G. Greco, E. Novellino, Perspect. Drug Dis. Des. 12 (1998) 257–315.
[29] J. Gasteiger, H. Saller, Angew. Chem.: Int. Ed. Engl. 24 (8) (1985) 687–689.